RSC Advances

ROYAL SOCIETY OF CHEMISTRY

www.rsc.org/advances

Influences of glycerin co-solvent on compatibility of MgAl hydrotalcites into polypropylene matrix

Hong-Yan Zeng*, Jin-Ze Du, Sheng Xu, Meng-Chen Liao, Xiao-Jun Liu, Heng-Zhi Duan, Chao-Rong Chen

School of Chemical Engineering, Xiangtan University, Xiangtan 411105, Hunan, China

*Corresponding Author

Hong-Yan Zeng

E-mail address: hongyanzeng99@hotmail.com; hyzeng@xtu.edu.cn

Address: School of Chemical Engineering, University of Xiangtan, Xiangtan 411105, Hunan, China

Tel.: 86-731-58298175

Fax: 86-731-58298167

Abstract

Hydrotalcites as flame retardants for industrial applications requires good compatibility with polymer. Glycerin co-solvent was employed during the precipitation of the MgAl hydrotalcites (Mg/Al-HT) particles and the dispersion of the Mg/Al-HT particles in polypropylene (PP) matrix was studied. The microstructures, textural and surface properties of the hydrotalcites were contrastively investigated by X-ray diffraction (XRD), scanning electron microscopy (SEM), fourier transform infrared spectra (FT-IR), laser particle size analyzer, barrett-joyner-hallender/brunauer-emmett-teller (BJH/BET), and thermogravimetric and differential thermal analysis (TG-DTA) as well as pH_{zpc} analyses. The results suggested that the interactions between the co-solvent and the Mg/Al-HT affected the nucleation, resulting in the variation of crystallinity. The employment of glycerin co-solvents during the nucleation was conducive to the combination of crystal water with the brucite sheets. The hydrotalcite (mix-MHT) obtained by adding glycerin co-solvent during the nucleation possessed the smallest particle sizes with the narrowest size distribution and highest hydrophobic surface of the particles, which made the mix-MHT particles to disperse uniformly throughout the PP matrix due to its good compatibility with PP. The improvement of the compatibility between the particles and polymer was mainly caused by the decrease of the hydrophily on the surface of the particles due to the presence of glycerin in the interlayer spaces of the mix-MHT particles. The employment of the mix-MHT particles into PP matrix could also significantly enhance the thermal stability, and maintain the mechanical properties of PP, and the mix-MHT had best performances as a flame retardant for PP matrix.

Keywords: glycerin; co-solvent; hydrotalcites; compatibility; PP matrix

1. Introduction

Due to the great demand of polymeric materials today, non-flammable or flame-retardant techniques are particularly craved, because most of the polymeric materials are easily burned. [1,2] Inorganic materials such as clays, $Al(OH)_3$ and $Mg(OH)_2$ have shown to improve the flame resistance, thermal, and mechanical properties of polymers. [3-5] The two inorganic materials, $Al(OH)_3$ and $Mg(OH)_2$, are now widely used as flame retardants, which have poor compatibility with polymer materials and need a very high loading (50~70 wt.%) to impart a good flame retardancy to polymer materials.[6] Of these clays, layered double hydroxides (HT) have received much attention because of their environmental friendliness, low cost, low toxicity and low smoke, [7,8] especially Mg/Al hydrotalcites (Mg/Al-HT) which have higher flame retardant effect than $Al(OH)_3$ or $Mg(OH)_2$ at the same loading level . [9,10] As compared to conventional materials, polymer/Mg/Al-HTs composites have more excellent mechanical properties, barrier, thermal stability and flame resistance properties. However, its flame retardant efficiency is still low due to high loading, for compatibility between the nonpolar polymers and Mg/Al-HT is poor and size of Mg/Al-HT particles large. [8,11,12] The challenges are the preparation of HT particles with smaller particle sizes, the homogeneous dispersion of inorganic material into the polymeric matrix and the compatibility of polymer/inorganic blends.

If the size of the crystallites and the Mg/Al-HT particles can be controlled during their synthesis, thus the prepared Mg/Al-HT will be better applied in the field. Some properties of the particles is modulated by the organic solvents, an effect which induces subtle changes in

microstructures and surface chemical properties of gel materials. [13] Four kinds of polyhydric alcohols including glycerin are employed as co-solvents to synthesize Mg/Al-HT respectively, and are found that polyhydric alcohols play an important influence on the microstructure and thermal stability of Mg/Al-HT synthesized using hydrothermal method. [14] The polyhydric alcohols can modify the surface and porosity properties of Mg/Al-HT, and synthetic routes effect on the properties, too. [15] All in all, the polyhydric alcohol co-solvents have a great influence on the preparation of the Mg/Al-HT, which affect the nucleation and subsequent crystal growth of the HT resulting in the variation of crystallinity and thermal stability. [14,15]

To make Mg/Al-HT particles smaller in size and with narrower size distribution as well as better compatibility, the present work demonstrated a new method of preparation to prepare the ultrafine Mg/Al-HT particles by glycerin as a co-solvent to control the nucleation or growth of the crystallites. The microstructure, morphology and surficial properties of the Mg/Al-HT particles were investigated by XRD, SEM, FT-IR, laser particle size analyzer, BJH/BET, DTA and pH_{zpc} analyses. The Mg/Al-HT particles were incorporated into polypropylene (PP) to obtain PP/Mg/Al-HT composites in order to improve flame retardant properties of the PP matrix.

2. Experimental

2.1. Materials

Polypropylene particles (K8303, melt flow rate: 2.6g·10 min^{-1} at 230°C and 2.16 kg) with the particle size about 1 mm, were purchased from Yanshan Petrochemical I Co., Ltd. (Beijing, China). All chemicals were of analytical grade, which was purchased from Sinopharm

Chemical Reagent Co. Ltd., China. All other reagents used in the experiment were of analytical grade, and all the solutions were made with deionized water.

2.2. Preparation of Mg/Al-HT

The hydrotalcite (Mg/Al-HT) with Mg/Al molar ratio of 3.0 was prepared by urea method (urea/NO_3^- molar ratio of 3.0). [16] The precipitation of the Mg/Al-HT particles could be divided into two steps: nucleation and crystallization. Firstly (nucleation), the mixed salt solution containing of $Mg(NO_3)_2 \cdot 6H_2O$ (0.12 $mol \cdot L^{-1}$), $Al(NO_3)_3 \cdot 9H_2O$ (0.04 $mol \cdot L^{-1}$) and urea was placed into a three-neck flask. The solution was maintained at 105°C for 10 h under stirring (300 rpm). Secondly (crystallization), it was then crystallized statically at 80°C for another 6 h. The solid was collected by filtration and washed to neutral using deionized water, and subsequently dried at 90°C for 24 h, which was denoted as AHT.

2.3. Preparation of Mg/Al-HT in co-solvent system

The preparation procedure by adding glycerin co-solvent was basically the same as above. The co-solvent solution was obtained by the addition of glycerin into the mixed salt solution with the volume ratio of 15 vol.%. When glycerin was adding into the mixed salt solution before the nucleation, the obtained solid sample was denoted as mix-MHT. When glycerin was adding into the salt mixed solution before crystallization, the obtained solid sample was denoted as bef-MHT. After crystallization, the solid was collected by filtration and washed to neutral using deionized water. The washed solid was again added into the co-solvent solution containing glycerin at 30°C for 90 min under stirring (300 rpm), and subsequently dried, which was denoted as aft-MHT.

2.4. Preparation of PP/ Mg/Al-HT composites

Polypropylene/mix-MHT (PP/mix-MHT) composite was prepared by melting, and then mixing the mix-MHT with PP matrix in a GH-10A high-speed mixer (Beijing Plastic Machinery Factory) with a rotor speed of 250 rpm at 230°C for 15 min. The mass loading of mix-MHT added (corresponding to pure PP) was 10 wt.%. The admixtures molded into bars (120×10×4 mm^3) using JK-WZM-I micro injection molding machine with a twin screw extruder (SHJ-30A) (Beijing Heng Odd Instrument Co., Ltd.) for the testing. The Polypropylene/AHT (PP/AHT) composite was used as a comparison.

2.5. Characterization

2.5.1. Characterization of Mg/Al-HT particles

X-ray diffraction (XRD) patterns were collected on a Rigaku D/max-2550PC (λ=1.5406 Å) with Cu Kα radiation. The scan step was 0.0671°/s with a filament intensity of 30 mA and a voltage of 40 kV. Scanning electron micrograph (SEM) images were obtained with a JEOL JSM-6700F instrument at an accelerating voltage of 10 kV. Fourier transform infrared (FT-IR) was recorded on Perkin-Elmer Spectrum One B instrument using KBr pellet technique. The particle size distribution was determined using a Malvern Mastersizer 2000 laser particle size analyzer. The pore size distribution was calculated from desorption isotherm by the barrett-joyner-hallender (BJH) method, and the specific surface area was calculated using the brunauer-emmett-teller (BET) method based on the N_2 adsorption isotherm from Quantachrome NOVA-2200e instrument. Thermogravimetric and differential thermal analysis (TG-DTA) was carried out in a nitrogen atmosphere with a Seiko 6300 TG-DTA instrument

with a heating rate of 10°C·min^{-1} under a He stream flowing at 60 mL·min^{-1}.

2.5.2. Characterization of PP/Mg/Al-HT composites

The phase morphologies of the PP/AHT and PP/mix-MHT composites were observed using SEM with an accelerating voltage of 25 kV. The specimen for the SEM observation was prepared by cryogenic fracture in liquid nitrogen, and the fracture surface was coated with a thin layer of gold before measurement. The TG analysis was performed using a Perkin-Elmer Pyris-1 TG-DTA instrument. 10 mg of the samples (PP, PP/AHT and PP/mix-MHT) were loaded in an open ceramic crucible, and heated in an air atmosphere at a heating rate of 10°·min^{-1}.

The impact strength was measured with a simple beam impact testing machine (XJJ-22) at room temperature based on the standard GB/T1043-1993 with 45° V-shaped notch and a notch-tip radius of 0.2 mm. Three specimens were repeated, and the average values in order to obtain reproducible results. And the other mechanical properties were measured using an electronic tensile test machine (RGD-5) with a crosshead speed of 30 mm·min^{-1}. Tensile strength, fracture elongation and fracture elongation were determined based on the standard GB/T1042-1992, GB/T1042-1992 and GB/T9341-2000, respectively. Three specimens at least were repeated to determine the average values in order to obtain reproducible results.

2.6. pH point of zero charge

The determination of the pH point of zero charge (pH_{zpc}) of the Mg/Al-HT particles was carried out using the potentiometric titration (PT) method described by Li et al. [17] The pH at

pH_{zpc} was determined in NaCl solutions (inert electrolytes) with different concentrations. The experiments were carried out in a shaker at 150 rpm and 25°C for 200 min. After the experiments, the pH in the solution was measured while a 0.1 $mol \cdot L^{-1}$ NaOH solution was added. The adsorption amount of H^+ (Γ_{H^+}) and OH^- (Γ_{OH^-}) was calculated. Finally, PT curves were obtained by plotting ($\Gamma_{OH^-} - \Gamma_{H^+}$) versus pH in NaCl solutions with different concentrations, and the crossover point of ($\Gamma_{OH^-} - \Gamma_{H^+}$) ~ pH_{zpc} curves was pH_{zpc}, which was electrically neutral. The permanent charge density (σ_p) at pH_{zpc} was as follow, [18]

$$\sigma_p = F(\Gamma_{OH^-} - \Gamma_{H^+})_{zpc} / S_{BET}$$

where, S_{BET} and F were specific surface area of the Mg/Al-HT particles and Faraday constant (96485 $C \cdot m^{-2}$), respectively.

3. Results and discussion

3.1. Characterization of Mg/Al-HT particles

3.1.1. XRD analyses

The powder XRD patterns for the AHT, mix-MHT, bef-MHT and aft-MHT samples are shown in Fig. 1. There is a typical layered double hydroxide structure with sharp and intense (003), (006), (009), (110) and (113) reflections and broadened (015) and (018) reflections in the samples. Further analysis of the XRD patterns reveals some differences in the cell parameters among the samples. The interlayer distances ($d_{003} \approx 0.76$ nm)(Table 1), in all the XRD patterns of the Mg/Al-HT samples, are typical of carbonated hydrotalcites.[19] No other crystalline phases are observed in the XRD patterns of all samples, indicating that the samples

are highly crystalline hydroxide structures. Especially, the d_{003} value (0.761 nm) of the mix-MHT is 0.006 nm higher than that of the AHT (0.755), which may have been due to the intercalation of glycerin. The interlayer distances of the bef-MHT (0.758 nm) and aft-MHT (0.753 nm) are the basic same as that of the AHT, which may be that the content of the glycerin molecules in the interlayer spaces is too small to detect them by XRD. The results show that the mix-MHT have the maximum interlayer distance due to having the highest amount of glycerin molecules in the interlayer spaces. The parameter *a*, average cation-cation distance in the brucite sheets, is calculated from the (110) XRD reflection in Table 1. The similarity in *a* value among the samples indicate that the addition of glycerin did not change the microstructure of the brucite sheets. The crystallite size in *a* direction (d_a) of the mix-MHT is smaller than that of other three samples, and the crystallite size in *c* direction (d_c) followed a similar trend, implying that the mix-MHT possesses the smallest crystallite size. The results reveal that glycerin co-solvent has little effect on the crystallinity of the Mg/Al-HT particles. However, glycerin added during the nucleation has impact on the crystallite size, which causes the crystallite size smaller.

3.1.2. SEM analyses

In order to investigate the morphology, the AHT, mix-MHT, bef-MHT and aft-MHT samples are observed by SEM analyses in Fig. 2. For all the samples, thin flat crystals indicating the layered structure are found in line with the typical hydrotalcite morphology with irregular edges. The mix-MHT is made up of individual platelet particles and there are little platelets to stack, while the particles of the AHT, bef-MHT and aft-MHT samples are slightly stacked in

all space directions forming some aggregates. The improvement the reunion of the mix-MHT particles may be explained that glycerin is added during the nucleation as a co-solvent rendering a decrease in the agglomeration. On the other hand, the particle sizes of the mix-MHT are significantly smaller than that of other three samples, where there are no significant differences in particle sizes among the AHT, bef-MHT and aft-MHT samples. The results indicate that glycerin added during the nucleation make the mix-MHT particles more diffuse, and at the same time the particle sizes are smaller, which is consistent with the inference provided by XRD analyses (Fig.1).

3.1.3. FT-IR analyses

The FT-IR spectra of the AHT, mix-MHT, bef-MHT and aft-MHT samples in the region 400~4000 cm^{-1} are displayed in Fig. 3, where the FT-IR spectra of the samples are typical of pure hydrotalcite structure and generally similar except for some minor differences. Absorption band at about 3446 cm^{-1} is attributed to the stretching vibrations (v_1−OH) of structural hydroxyl groups in the brucite sheets,[8] where the increase in intensity and shifts to lower wavenumber indicate a increase in the number of –OH group due to the addition of the glycerin.[14] There is a similarity of band width and shift (4 cm^{-1}) between the bef-MHT and aft-MHT, though it is wider than the band width of the ATH, implying that the bef-MHT and aft-MHT had glycerin molecules. The widest characteristic band with the highest shift (7 cm^{-1}) appeared in the mix-MHT indicates that the mix-MHT particles contain the most of glycerin molecules. The weak band appeared around 2956 cm^{-1}, attributed to the asymmetric stretching vibration of $–CH_2$, [14,20] can be observed in the mix-MHT, bef-MHT and aft-MHT,

where the intensity of the broad for the mix-MHT is obviously enhanced. The result shows that glycerin is presented in the three samples and the amount of glycerin in the mix-MHT is more than that of the bef-MHT or aft-MHT. The band appeared around 1386 cm^{-1} is resulted from the asymmetrical stretching vibration of CO_3^{2-},[11] and the bands in the mix-MHT, bef-MHT and aft-MHT split into two bands which is likely due to the existence of $-CH_2$. [21] The appearance of these bands suggests that glycerin molecules exist in the mix-MHT, bef-MHT and aft-MHT, and the mix-MHT has the highest amount of glycerin, which is in agreement with the results of XRD. The sharp absorption band at 1630 cm^{-1} is usually assigned to the bending vibration of the interlayer water or physically adsorbed water. [11] The bands at 780 and 553 cm^{-1}(Al-OH), 447 cm^{-1}($[AlO_6]^{3-}$, or Al-OH) and 686 cm^{-1}(Mg-OH) are clearly observed in the spectra of all the samples, too.

3.1.4. Particle size, BJH and BET analyses

The particle size distribution and the average particle sizes for all the samples are illustrated in Fig. 4. The most probable sizes of the AHT, mix-MHT, bef-MHT and aft-MHT particles are approximately 0.45, 0.98, 1.87 and 5.9 μm, respectively. The most probable size distribution with 90% of particles is found in the range of 0.08~1.45 μm for the mix-MHT, whereas it is found in the range of 0.8~11.5 μm for the AHT. There is a same size distribution of the bef-MHT and aft-MHT, which is in the range of 0.31~5.7 μm. The mix-MHT has the most uniform and smallest particle sizes comparing with the other three samples, while the bef-MHT and aft-MHT samples possess a narrower size distribution and smaller particle sizes than the AHT. It can be speculated that the reduction of the particles agglomeration is due to the presence of glycerin. The Mg/Al-HT particles with the most probable size distribution of

2~20 or 2~8 μm can be obtained using urea method, [22,23] while the size distribution and sizes in the range of 1~120 μm is obtained using co-precipitation.[24] The most probable size distribution and particle sizes of the mix-MHT are obviously narrower and smaller than those reported in the literature, respectively. The results indicate that the use of glycerin as co-solvent can prepare ultrafine hydrotalcites, and the mix-MHT has the most uniform and smallest particle sizes due to the most amount of glycerin, for the addition of glycerin as co-solvent before nucleation could give hydrotalcite particles more glycerin molecules.

On the other hand, the specific surface area, average pore diameter and pore volume of the samples are also investigated, and the results shown in Table 2. There are no significant differences or changes in average pore diameters and pore volumes among all the samples, implying that the use of glycerin co-solvent cannot impact the textural structure of the Mg/Al-HT particles. The phenomenon further verified the result of XRD that the structure of the brucite sheets do not change using glycerin co-solvent (Table 1). The mix-MHT has the highest specific surface area (S_{BET}, 96.71 $m^2 \cdot g^{-1}$) and lowest permanent charge density (σ_p, 1.12 $C \cdot m^{-2}$), followed by the bef-MHT and aft-MHT with permanent charge density σ_p of 1.87 and 1.51 $C \cdot m^{-2}$, respectively. The AHT possesses the lowest specific surface areas, exhibiting the highest σ_p with 2.95 $C \cdot m^{-2}$. Thus, there is reason to believe that glycerin molecules can increase the specific surface area by decreasing the particle sizes which is in agreement with the deduction of XRD and SEM analyses that the more amount of glycerin molecules is in the particles, the smaller the particle sizes are.

3.1.5. pH point of zero charge analyses

The point of zero charge (pH_{zpc}) was used in the determination of the surface charge properties of materials. As seen in Fig. 5, the pH_{zpc} value of the AHT is the highest at 2.42, followed by that of the bef-MHT and aft-MHT, and the pH_{zpc} value of the mix-MHT is the lowest at 1.84. The decrease in pH_{zpc} and σ_p demonstrates that the surface of the Mg/Al-HT particles becomes more negative, leading to a higher electrostatic repulsion between the particles.

3.1.6. TG-DTA analyses

Fig. 6 shows the TG-DTA curves of the AHT, mix-MHT, bef-MHT and aft-MHT particles. The DTG curves of the three samples (mix-MHT, bef-MHT and aft-MHT) are basically similar, but there are significant differences between the three samples and AHT. The DTA curve of the AHT shows two endothermic peaks, where the first peak is at 193°C due to the loss of the surface and interlayer water, and the second peak is at 393°C corresponding to the decomposition of CO_3^{2-} and dehydroxylation in layers. [25] However, the curves of the mix-MHT, bef-MHT and aft-MHT show three endothermic peaks. The first peaks of the AHT, mix-MHT, bef-MHT and aft-MHT are at 193, 245, 230 and 218°C, respectively. The increase of temperature at the first endothermic peak reveals the strengthening interaction, and the removal of water molecules becomes more difficult. So, for the AHT particles prepared in pure water, the hydration level is the lowest, and the crystal water is easy to release out. While for the mix-MHT, bef-MHT and aft-MHT particles, especially for mix-MHT, the release of the crystal water becomes the most difficult due to the strongest hydrogen bonding interaction. A similar trend in the temperature change at second endothermic peaks (393°C) is also found.

The increase in the decomposition temperature of CO_3^{2-} and –OH at 393°C is due to the presence of glycerin molecules, too. For the mix-MHT, bef-MHT and aft-MHT, the new weak endothermic peak at 320°C may be due to the effect of glycerin, which is associated with some complex process such as the decomposition of CO_3^{2-} in the interlayers and –OH in the brucite sheets held with different strengths due to intercalation of glycerin molecules. The weight losses at the new peak for the mix-MHT, bef-MHT and aft-MHT are 23.6%, 22.5% and 21.6%, respectively, implying that the mix-MHT contains the most amount of glycerin molecules. The result confirms that the mix-MHT has a maximum quantity of glycerin molecules in the interlayer spaces, which is already demonstrated by the XRD and FT-IR that has the highest amount of glycerin molecules (Fig.1 and Fig. 3). This may be because more glycerin molecules are intercalated into the interlayer spaces companying water molecules and CO_3^{2-} during the nucleation, while only a small amount of glycerin molecules can insert into the spaces before or after the crystallization.

According to the above analysis result, it is evident that glycerin co-solvent limits the growth of the HT particles leading to a reduction in the particle sizes and the size distribution narrowing, and imparts the hydrophobicity of the particle surface, so that the particles were repelled from each other due to electrostatic force. In particular, the employment of glycerin during the nucleation benefited the interaction between crystal water and brucite sheets, the more glycerin molecules entering the interlayer spaces, and the higher the hydration level, which can make the Mg/Al-HT particles to become smaller in the particle sizes and more hydrophobic. Based on the results of the experiments, the mix-MHT sample was chosen to investigate the dispersion of hydrotalcite particles into PP matrix.

3.2. Characterization of PP/Mg/Al-HT

3.2.1. SEM analysis of PP/Mg/Al-HT composites

The effect of blending the mix-MHT (10 wt.%) with PP matrix was evaluated from SEM images by cryo-fractured surfaces of PP/mix-MHT composites, which is presented in Fig. 7. The mix-MHT particles as pointed by white arrows are dispersed uniformly throughout the PP matrix. However, the AHT particles in the PP/AHT composite are badly agglomerated as white platelets as pointed by the white arrow. The particle sizes of the AHT are much greater than those of the mix-MHT. The result show that the employment of glycerin during the nucleation can improve the homogeneous dispersion of the Mg/Al-HT particles in PP matrix. Thus, the glycerin added during the nucleation can act as a co-solvent and promote the mix-MHT particles to disperse homogeneously in the PP matrix, namely improving compatibility.

3.2.2. Thermal Behavior of PP/Mg/Al-HT composites

The thermal decomposition temperatures of the PP/AHT and PP/mix-MHT composites are shown by the TG curves (Fig. 8). Compared to PP, the addition of Mg/Al-HT particles increased the thermal stability, but do not affect the degradation steps of the PP matrix. The effect of Mg/Al-HT on thermal stability of PP matrix can be compared by the two temperatures, namely onset decomposition temperature ($T_{0.1}$) and decomposition temperature ($T_{0.5}$), which are significantly increased with the presence of the Mg/Al-HT particles (Table 3). The PP/mix-MHT exhibits higher decomposition temperatures than the PP/AHT due to higher compatibility with PP matrix, indicating that the PP/mix-MHT possesses higher thermal

stability. The incorporation of glycerin during the nucleation can enhance the thermal stability of the PP/mix-MHT. Comparing with the AHT, the mix-MHT has smaller particle sizes, larger specific surface area and higher hydrophobicity, which makes it higher thermal stability and flame retardant properties of the PP/mix-MHT composite.

3.2.3. Mechanical Properties

The mechanical properties of the PP/AHT and PP/mix-MHT composites are revealed in Table 3. The employment of Mg/Al-HT particles into PP matrix has a small effect on the mechanical properties of PP. Among them, the PP/mix-MHT demonstrates the highest flexural strength, impact strength and tensile strength. The reinforcing mechanical properties of the PP/mix-MHT may be caused by higher compatibility and dispersion with the polymer from the more ultrafine particles as well as higher hydrophobicity outside comparing with the PP/AHT.

4. Conclusions

In order to obtain better dispersion and compatibility of hydrotalcites into PP matrix, the Mg/Al-HT were prepared using as glycerin co-solvent by a urea method. The samples were characterized by XRD, SEM, FT-IR, laser particle size analyzer, BJH/BET, DTA and pH_{zpc} analyses. It was found that the hydrophilic nature of the Mg/Al-HT particles was reduced, and the particle sizes was declined, consequently promoted diffusion of the particles in the PP matrix. Specifically, the incorporation of glycerin during the nucleation was found to be an effective method to obtain smaller and more hydrophobic Mg/Al-HT particles (the mix-MHT) that could be evenly dispersed into the PP/the mix-MHT composites to improve thermal

stability and keep the mechanical properties for PP matrix.

Acknowledgments

This work is supported by the Key Project of Hunan Provincial Natural Science Foundation of China (12JJ2008), Open Project of Hunan Provincial University Innovation Platform (12K048), Xiangtan University Graduate Innovation Project (XJCX201405) .

References

1. A. Blum, *Science*, 2007, **318**, 194-195.
2. P. Webster, *Science*, 2004, **304**, 1730.
3. P. Kiliaris, C. D. Papaspyrides, *Prog. Polym. Sci.*, 2010, **35**, 902-958.
4. J. Ma, J. Yang, Y. Huang, K. Cao, *J. Mater. Chem.*, 2012, **22**, 2007-2017.
5. Z. Wang, X. Shen, W. Fan, Y. Hu , B. Qu , Z. Gui, *Polym. Int.*, 2002, **51**, 653-657.
6. Y. Gao, Q. Wang, J. Wang, L. Huang, X. Yan, X. Zhang, Q. He, Z. Xing, Z. Guo, *ACS Appl. Mater. Interfaces*, 2014, **6**, 5094-5104.
7. W. Chen, B. Qu, *Chem. Mater,* 2003, **15**, 3208-3213.
8. H. Y. Zeng, P. H. Zhu, S. Xu, M. C. Liao, Z. Q. Zhang, X. J. Liu, J. .Z. Du, *Ind. Eng. Chem. Res*., 2014, **53**, 18380-18389.
9. L. Du, B. Qu, Z. Xu, *Polym. Degrad. Stabil.*, 2006, **91**, 995-1001.
10. C. Jiao, Z. Wang, X. Chen, B. Yu, Y. Hu, *Radiat. Phys. Chem.*, 2006, **75**, 557-563.
11. S. Xu, M. C. Liao, H. Y. Zeng, Z. Q. Zhang, X. J. Liu, P. H. Zhu, *Appl. Clay Sci.,* 2015, **108**,215-221.
12. M. Alexandre, P. Dubois, *Mat. Sci. Eng. R.,* 2000, **28**, 1-63.
13. A. R. Hirst, D. K. Smith, *Langmuir,* 2004, **20**, 10851-10857.
14. J. Wang, Y. Wei, J. Yu, *Appl. Clay Sci.,* 2013, **72**, 37-43.
15. F. Malherbe, C. Forano, J. P. Besse, *Micropor. Mat.,* 1997, **10**, 67-84.

16. H. Y. Zeng, X. Deng, Y. J. Wang, K. B. Liao, *AIChE. J*., 2009, **55**, 1229-1235.

17. S. P Li, W. G. Hou, S. H. Han, L. F. Li, W. Zhao, *J. Colloid Interf. Sci.*, 2003, **257**, 244-249.

18. W. G. Hou, Y. L. Su, D. J. Sun, C. G. Zhang, *Langmuir,* 2001, **17**, 1885-1888.

19. H. Y. Zeng, S. Xu, M. C. Liao, Z. Q Zhang, C. Zhao, *Appl. Clay Sci*., 2014, **91**, 16-24.

20. D. Basu, A. Das, K. W. Stöckelhuber, U. Wagenknecht, G. Heinrich, *Prog. Polym. Sci.,* 2014, **39**, 594-626.

21. T. Ishioka, K. Maeda, I. Watanabe, S. Kawauchi, M. Harada, *Spectrochim. Acta A*., 2000, **56**, 1731-1737.

22. M. Ogawa, H. Kaiho, *Langmuir,* 2002, **18,** 4240-4242.

23. X. Lei, F. Zhang, L. Yang, X. Guo, Y. Tian, S. Fu, F. Li, D. G. Evans, X. Duan, *AIChE. J.*, 2007, **53**, 932-940.

24. W. Xie, H. Peng, L. Chen, *J. Mol. Catal. A-Chem*., 2006, **246**, 24-32.

25. V. Rives, *Mater Chem. Phys.*, 2002, **75**, 19-25.

Figure legends:

Fig. 1 XRD patterns of the AHT, mix-MHT, bef-MHT and aft-MHT particles.

Fig. 2 SEM images of the AHT, mix-MHT, bef-MHT and aft-MHT particles, ×10 000.

Fig. 3 FT-IR spectra of the AHT, mix-MHT, bef-MHT and aft-MHT particles.

Fig. 4 Particle size distributions of the AHT, mix-MHT, bef-MHT and aft-MHT particles.

Fig. 5 PT curves of the AHT, mix-MHT, bef-MHT and aft-MHT particles.

Fig. 6 TG-TGA profiles of the AHT, mix-MHT, bef-MHT and aft-MHT particles.

Fig. 7 SEM images of the PP/AHT and PP/mix-MHT composites, ×500. White arrow pointing to the Mg/Al-HT particles in the composites.

Fig. 8 TG curves of the PP/ AHT and PP/mix-MHT composites.

Fig. 1

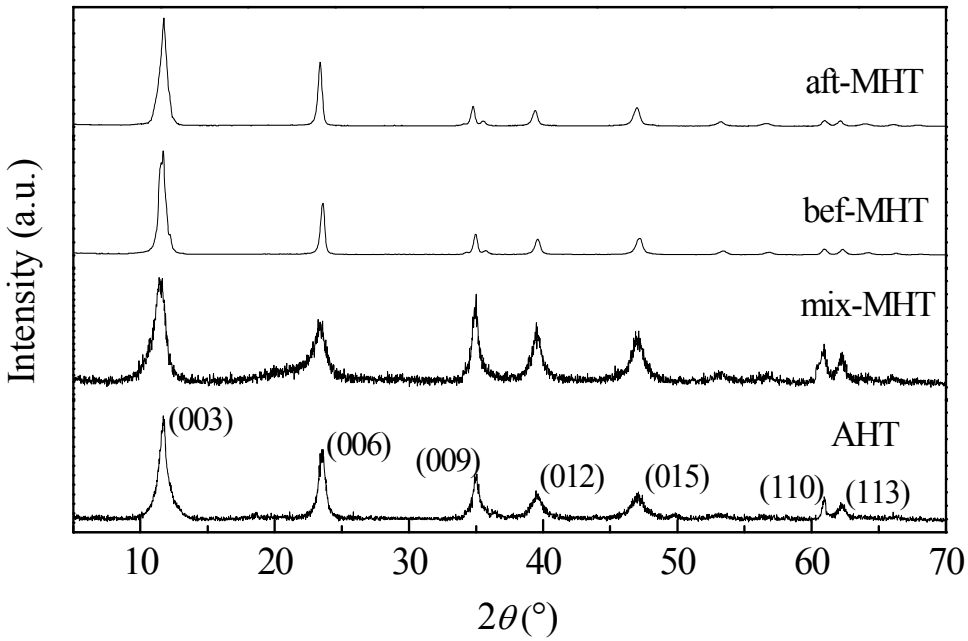

Fig. 2

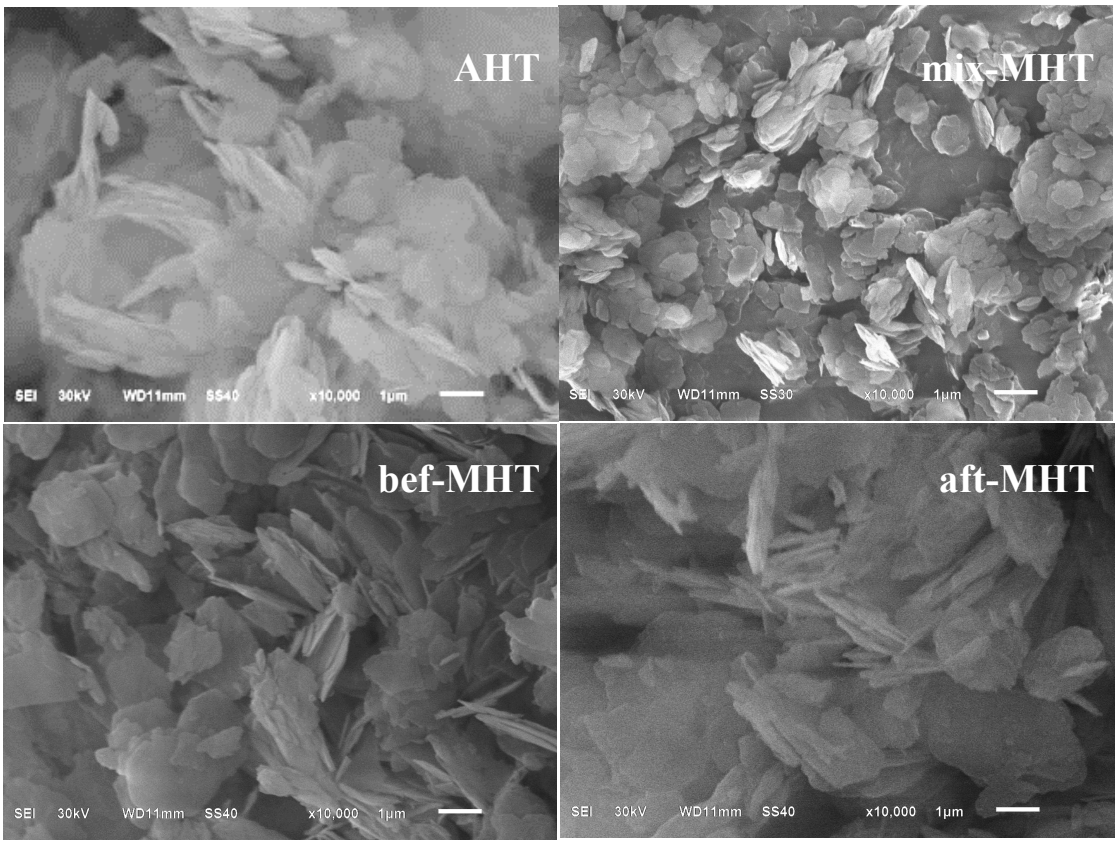

Fig. 3

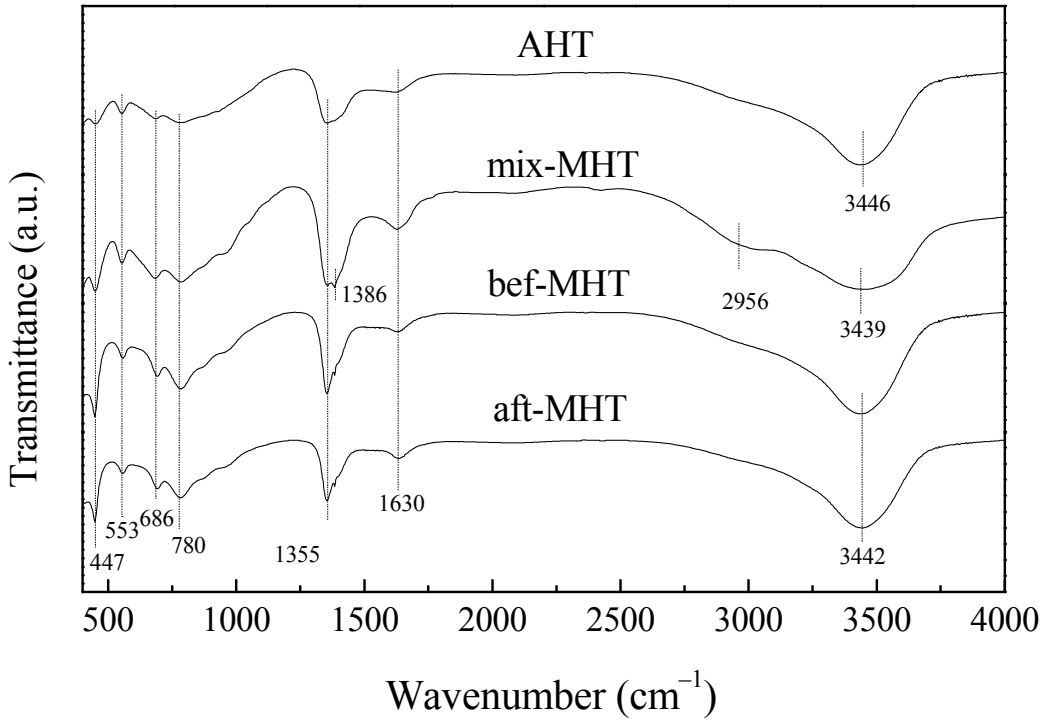

Fig. 4

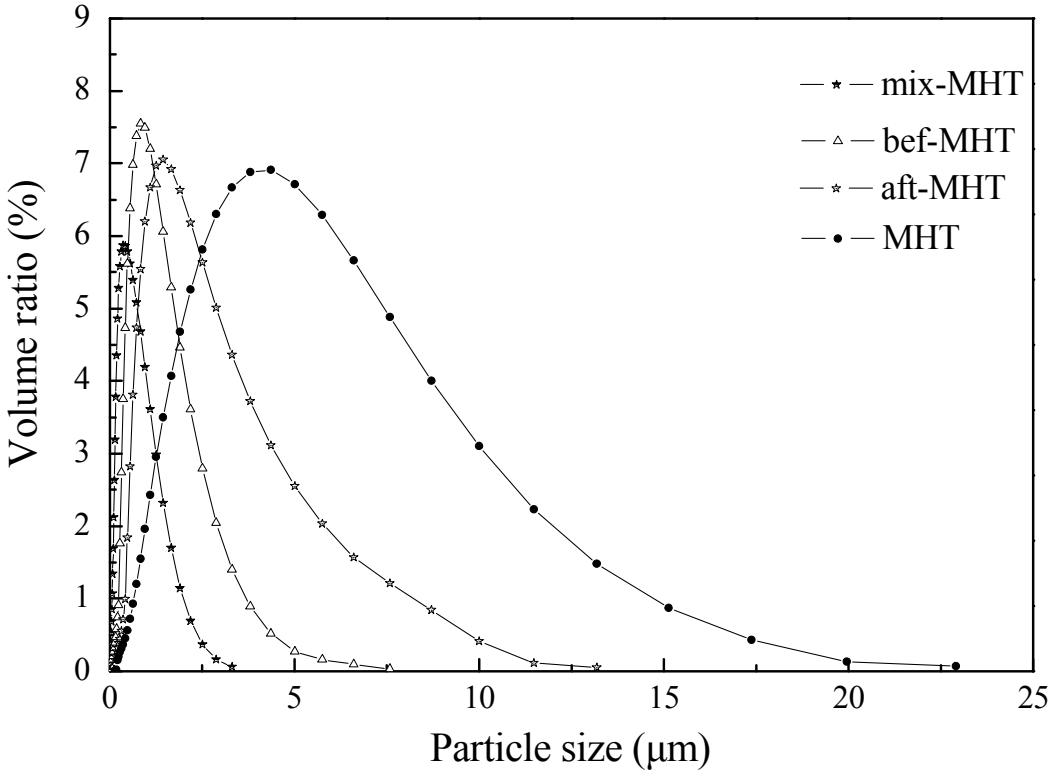

Fig. 5

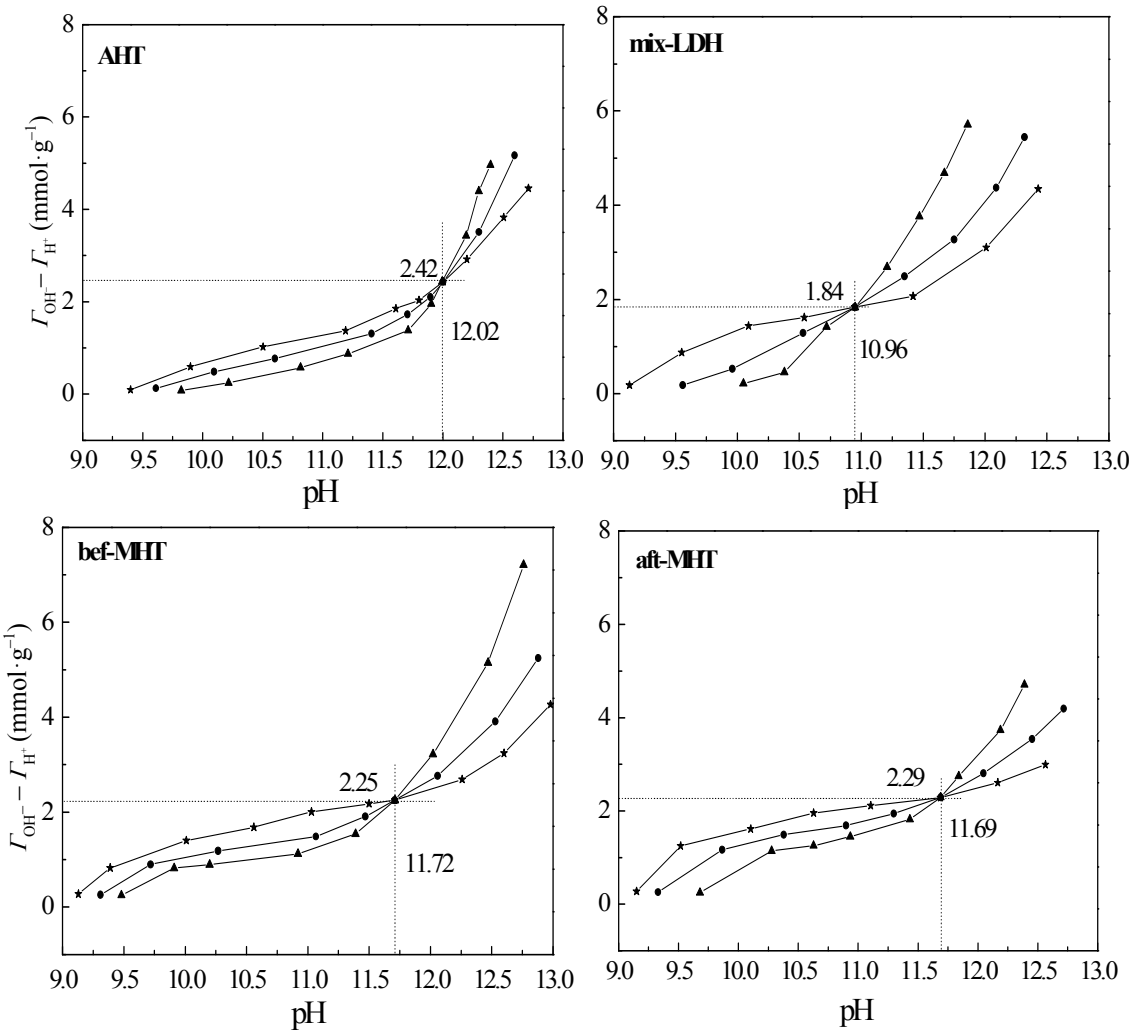

Fig. 6

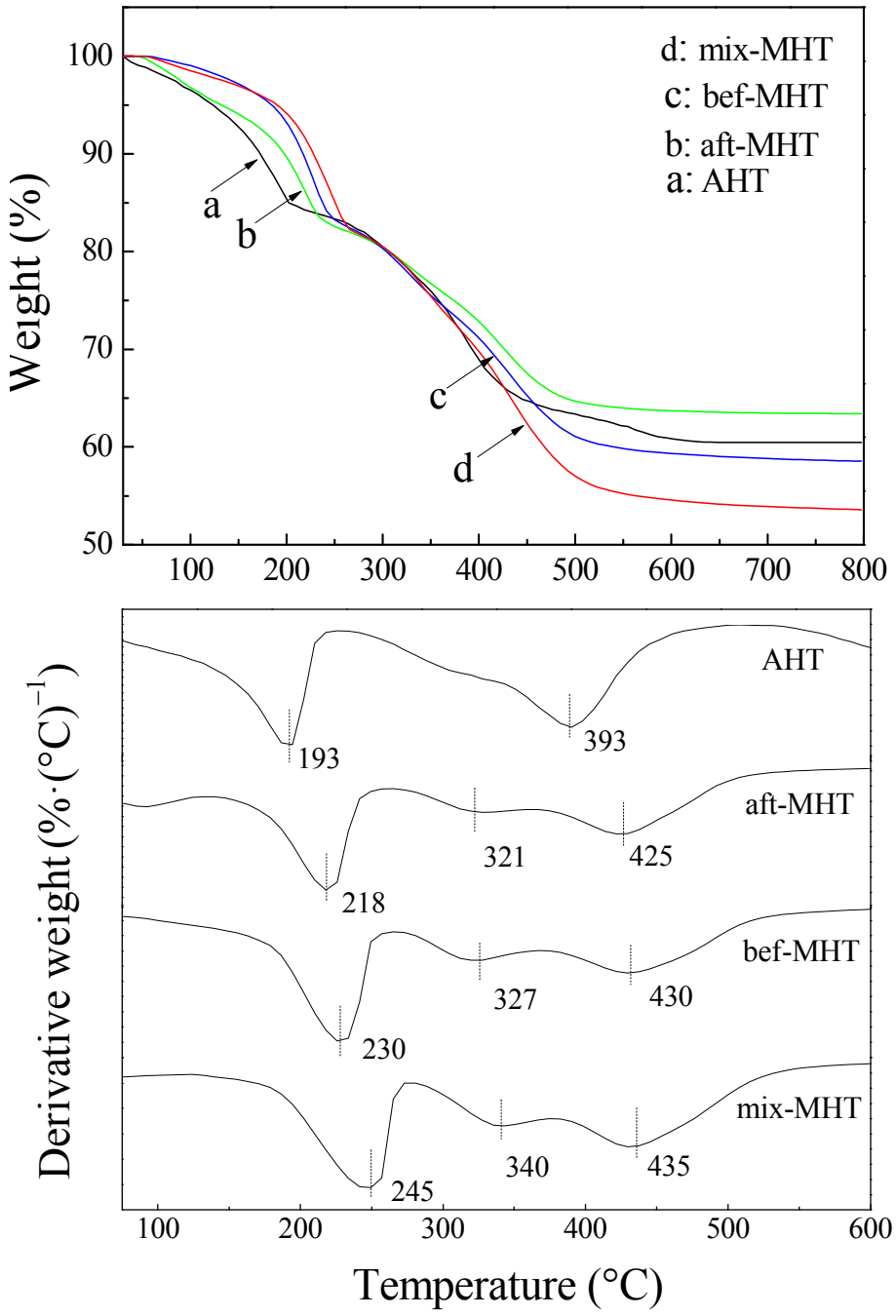

Fig. 7

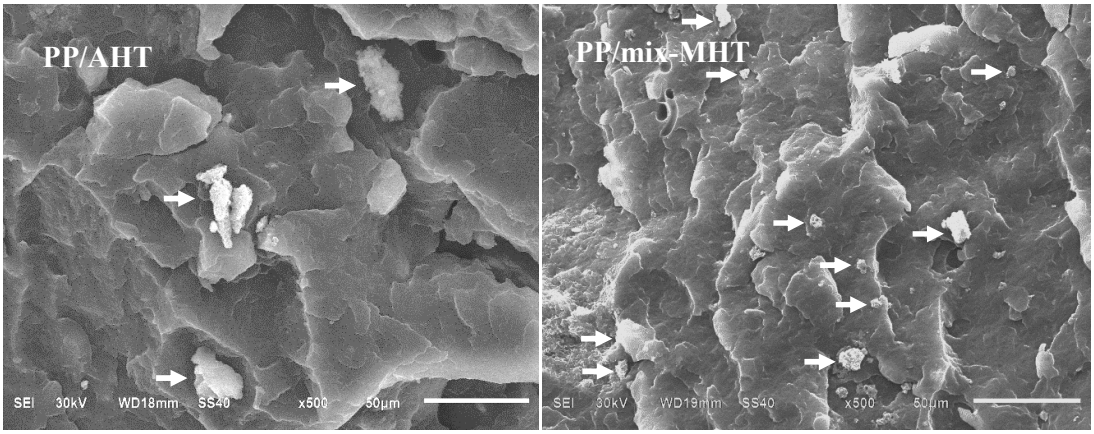

Fig. 8

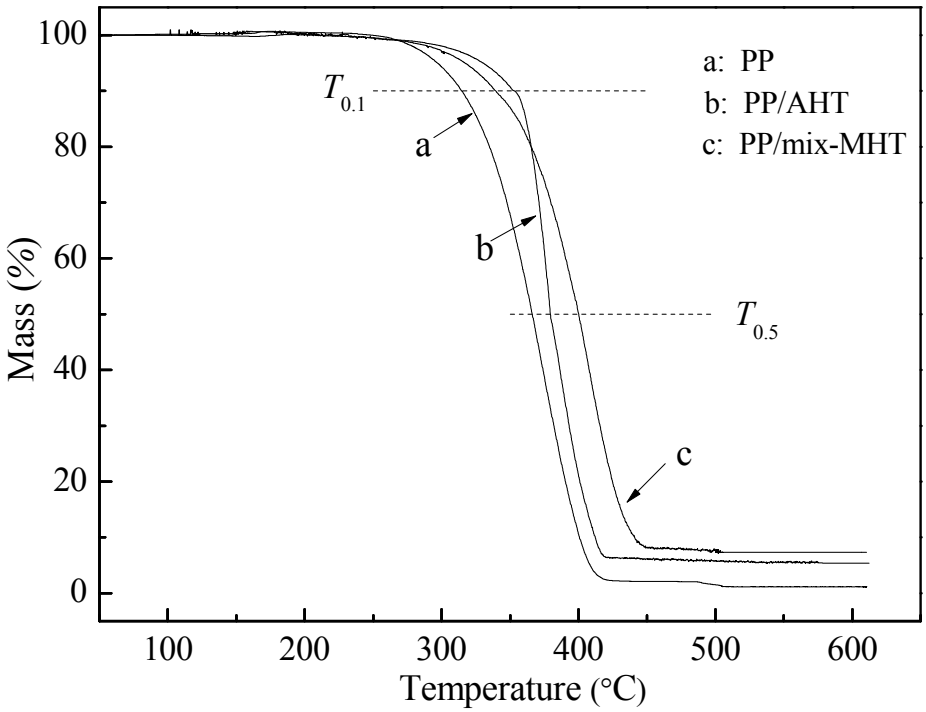

Table 1 Crystallographic parameters of the samples

Parameter	mix-MHT	bef-MHT	aft-MHT	AHT
d_{003} (nm)	0.761	0.758	0.753	0.755
d_{006} (nm)	0.380	0.377	0.377	0.376
d_{009} (nm)	0.256	0.256	0.262	0.255
d_{110} (nm)	0.152	0.152	0.152	0.152
FW_{003} (rad)	0.763	0.564	0.559	0.608
FW_{110} (rad)	0.349	0.406	0.384	0.383
a (nm)	0.304	0.304	0.303	0.303
c (nm)	2.292	2.280	2.293	2.268
S_c(nm)	10.36	14.02	14.15	13.99
S_a(nm)	21.68	22.48	22.59	22.53

FW: Half-width of diffraction peak; S_a: Crystallite size in a axis direction; S_c: Crystallite size in c axis direction.

Table 2 particle size distribution, textural properties and σ_p of the samples

Samples	S_{BET}($m^2 \cdot g^{-1}$)	Pore volume ($mL \cdot g^{-1}$)	Average pore diameter(nm)	σ_p ($C \cdot m^{-2}$)
AHT	75.16	0.296	3.821	2.95
mix-MHT	96.71	0.294	3.775	1.12
bef-MHT	87.81	0.244	3.774	1.87
aft-MHT	80.32	0.192	3.828	1.51

Table 3. Thermal stability and mechanical properties of PP/Mg/Al-HT composites.

Samples	PP	PP/AHT	PP/mix-MHT
$T_{0.1}$ (°C)	314.6	352.3	339.1
$T_{0.5}$ (°C)	365.8	379.4	400.2
Impact strength(kJ·m^{-2})	5.646	5.821	5.925
Tensile strength (MPa)	23.87	23.21	25.87
Flexural strength (MPa)	46.08	48.50	50.01
Fracture elongation (%)	37.69	31.43	34.43